Validation of non-REM sleep stage decoding from resting state fMRI using linear support vector machines

Altmann A.[1,2,7]*, Schröter M.S. [1,3]*, Spoormaker V.I.[1], Kiem S.A.[1], Jordan D.[4], Ilg R.[5,6], Bullmore E.T.[3], Greicius M.D.[2], Czisch M.[1], Sämann P.G.[1]

*equal contribution

[1] Max Planck Institute of Psychiatry, Department of Translational Research in Psychiatry, Neuroimaging, Munich, Germany

[2] Stanford Center for Memory Disorders, Department of Neurology and Neurological Sciences, Stanford University, Stanford, CA, USA

[3] Behavioural and Clinical Neuroscience Institute, Department of Psychiatry, University of Cambridge, Cambridge, United Kingdom

[4] Department of Anesthesiology, Klinikum rechts der Isar, Technische Universität München, Munich, Germany

[5] Department of Neurology, Klinikum rechts der Isar, Technische Universität München, Munich, Germany

[6] Asklepios Stadtklinik, Bad Tölz, Germany

[7] Present address: Translational Imaging Group, Centre of Medical Image Computing, University College London, London, UK

Short title: 'Resting state fMRI predicts sleep'

Key Words: resting state fMRI, EEG, EEG-fMRI, sleep, classification

Corresponding author: Andre Altmann

Translational Imaging Group

4 Stephenson Way

NW1 2HE, London, United Kingdom

E-mail: a.altmann@ucl.ac.uk

Phone: +44 7758 542270

Number of figures and tables: 5 figures, 1 table

Contents of supplemental material: 10 figures, 2 tables

Supplementary Information

Figure S1: **Classifier performance on individual tasks with training and validation data being swapped.** Here, the roles of the training and validation dataset were swapped, i.e., LOSO-CV was carried out on the validation data and the larger training datasets acted as an independent validation dataset. Note that due to a lack of instances of SW in the validation dataset, these respective classifiers could not be trained.

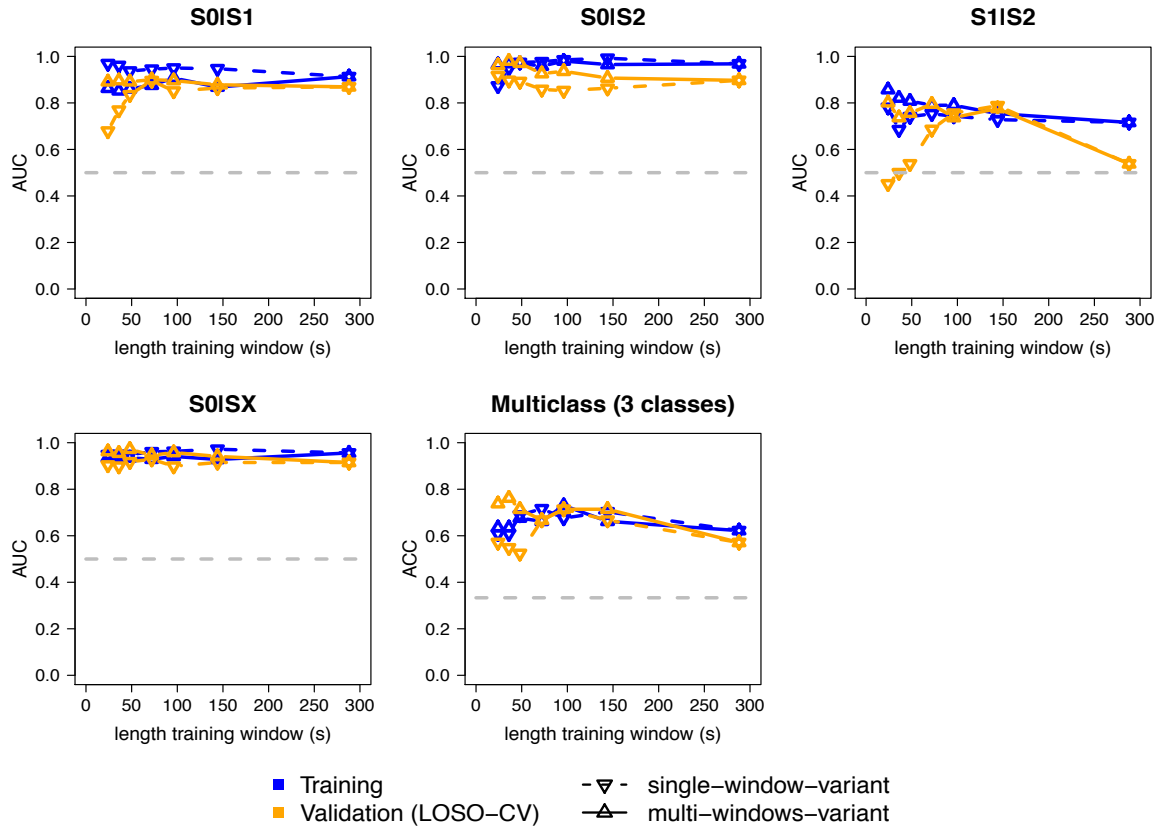

Figure S2: **Visualization of the most discriminant connections for S0|S1.** Same as Figure 4, but all 200 connections with a permutation p-value of 0.05 and lower are depicted.

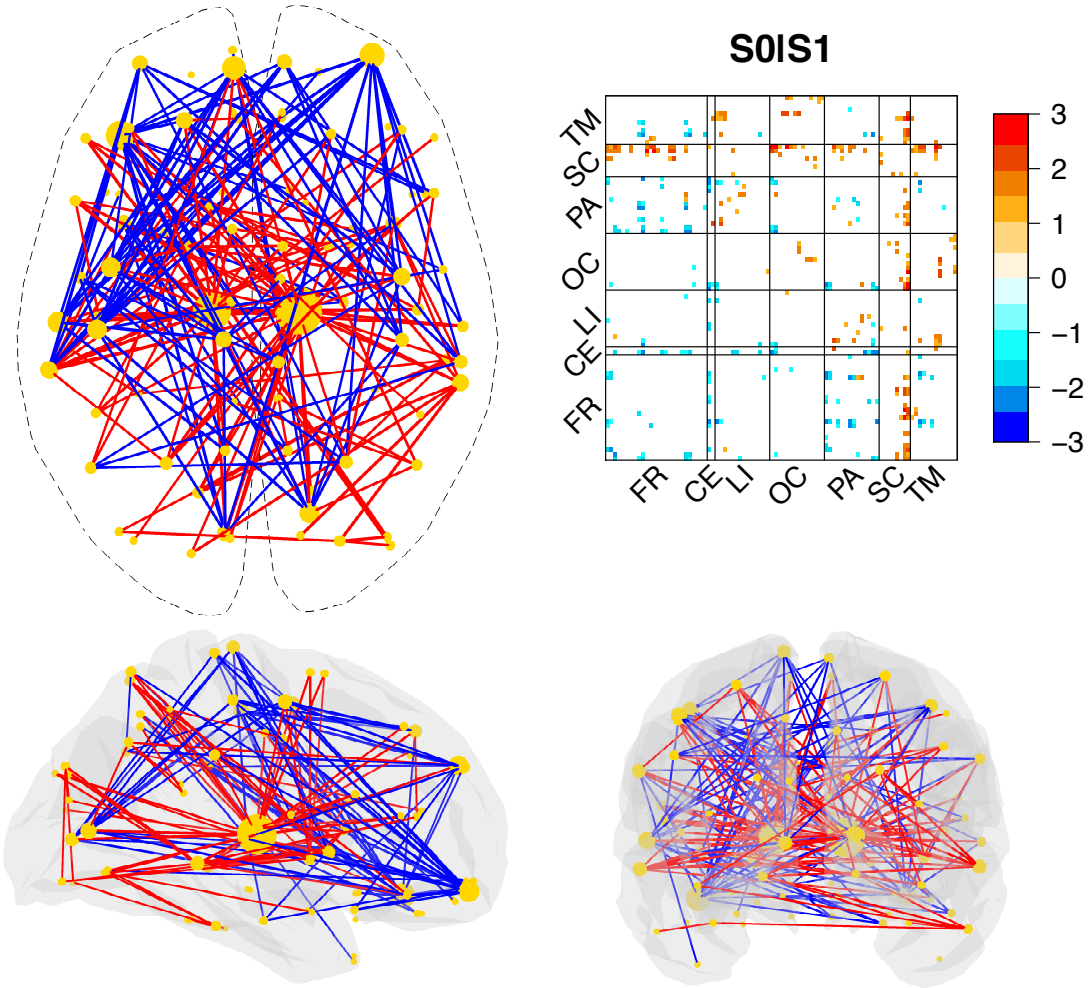

Figure S3: **Visualization of the most discriminant connections for S0|S2.** Same as Figure 4, but for S0|S2 with a permutation p-value threshold of 0.01.

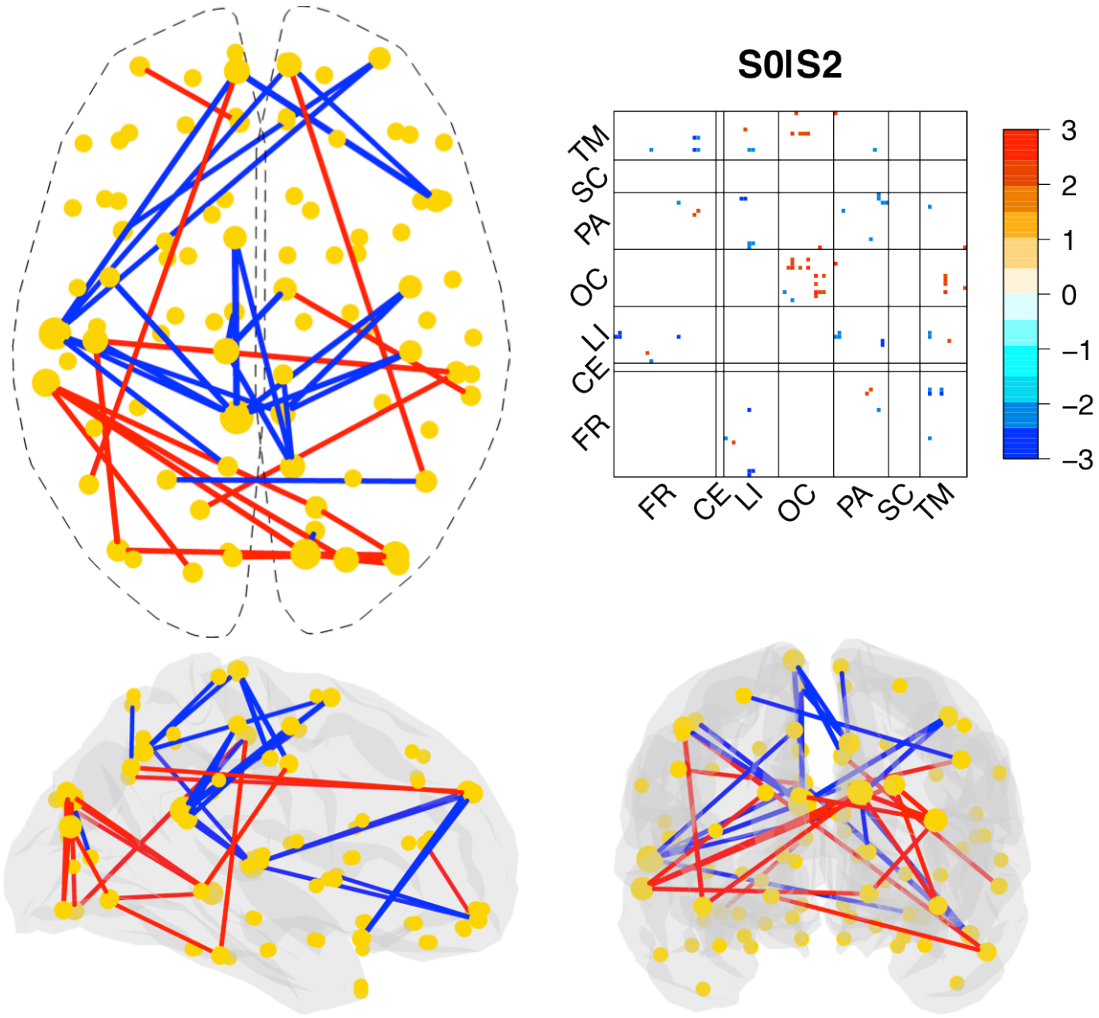

Figure S4: **Visualization of the most discriminant connections for S0|SW.** Same as Figure 4, but for S0|SW with a permutation p-value threshold of 0.01.

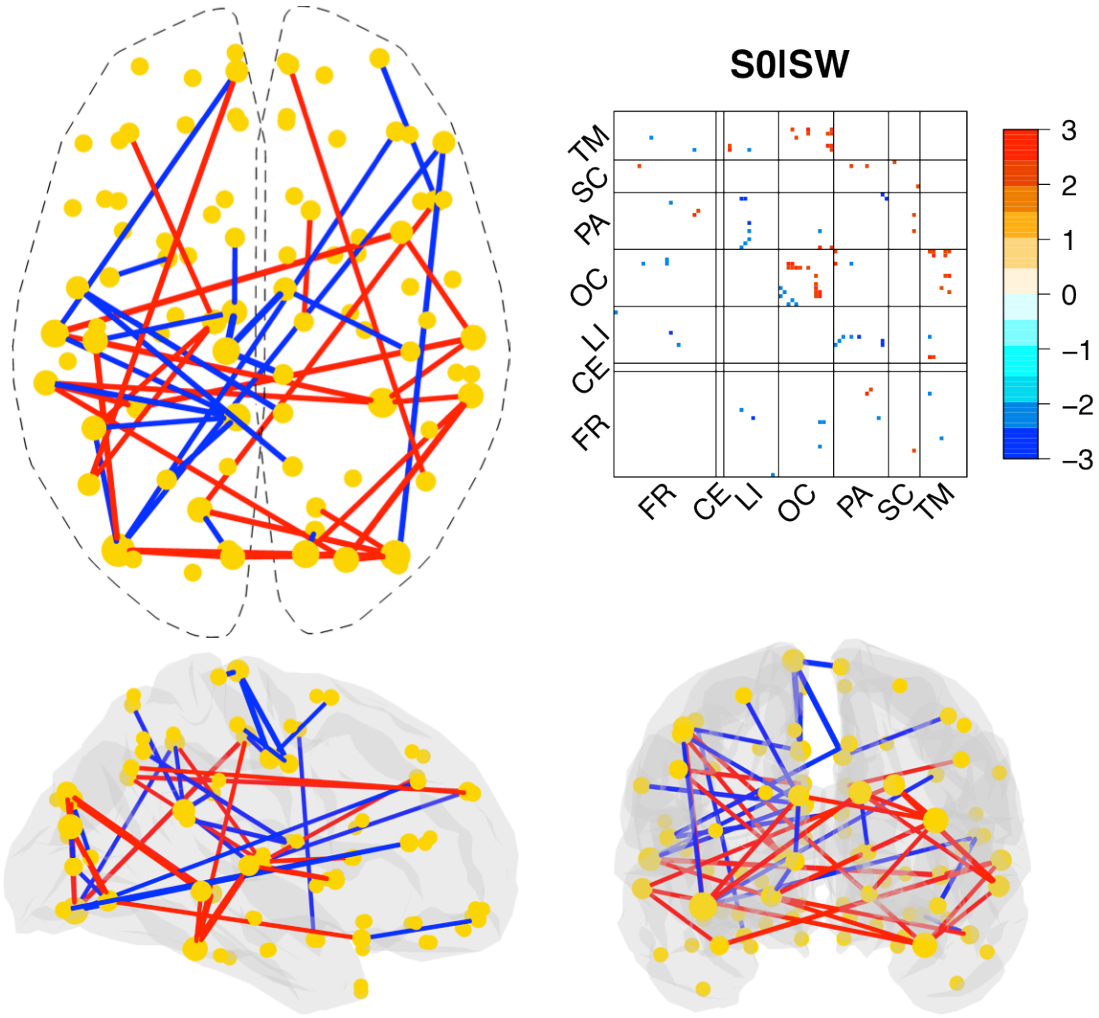

Figure S5: **Visualization of the most discriminant connections for S1|SW.** Same as Figure 4, but for S1|SW with a permutation p-value threshold of 0.01.

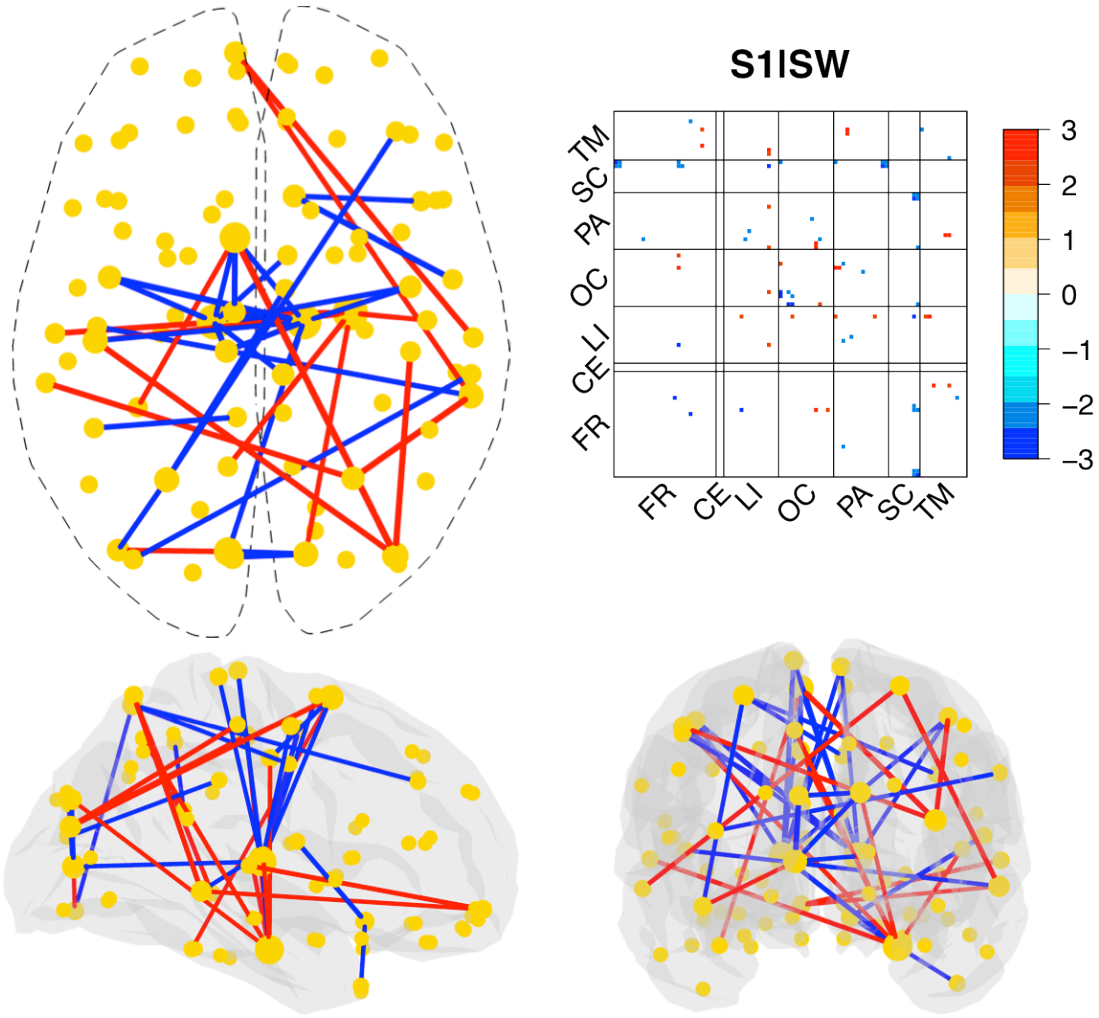

Figure S6: **Distribution of ICI and RCI.** Each panel depicts the distribution of ICI and RCI for each class.

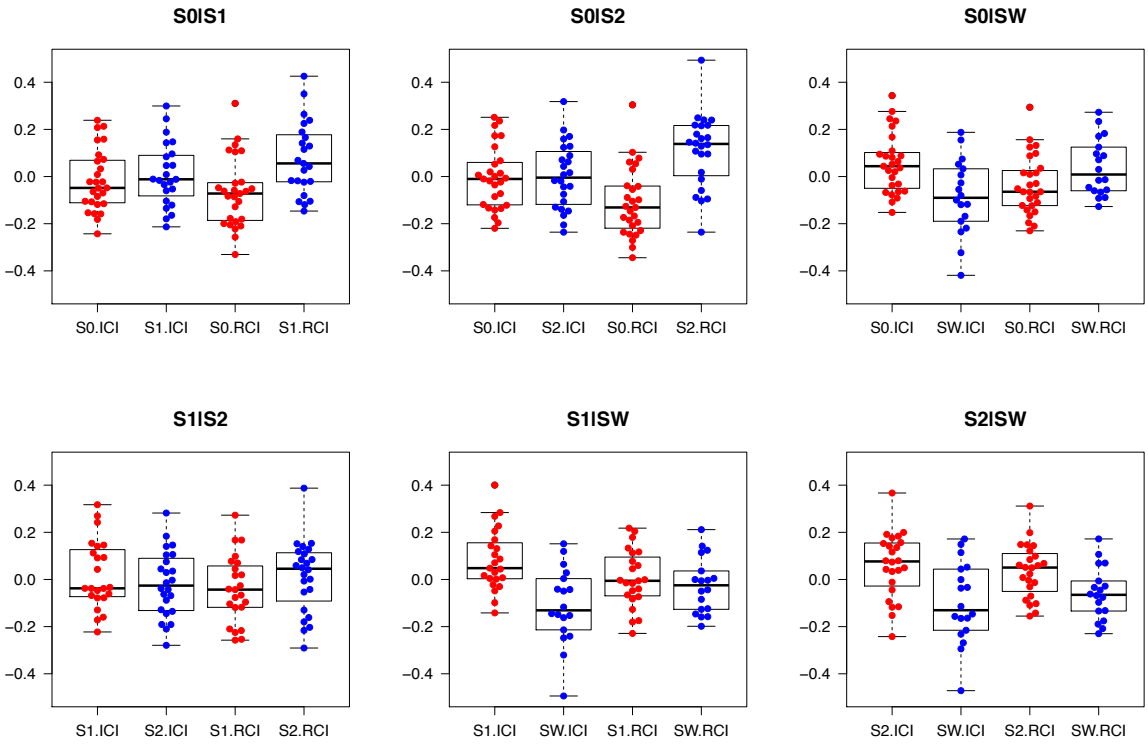

Figure S7: **Increased and reduced connectivity index for the four binary classification tasks on the validation dataset.** Same as Figure 5, but depicted epochs originate from the independent test data. Epochs are colored according to the EEG based sleep stage: black (S0), red (S1), and blue (S2). The panel S0|SX shows the ICI and RCI representation of the classifier separating wakefulness from sleep.

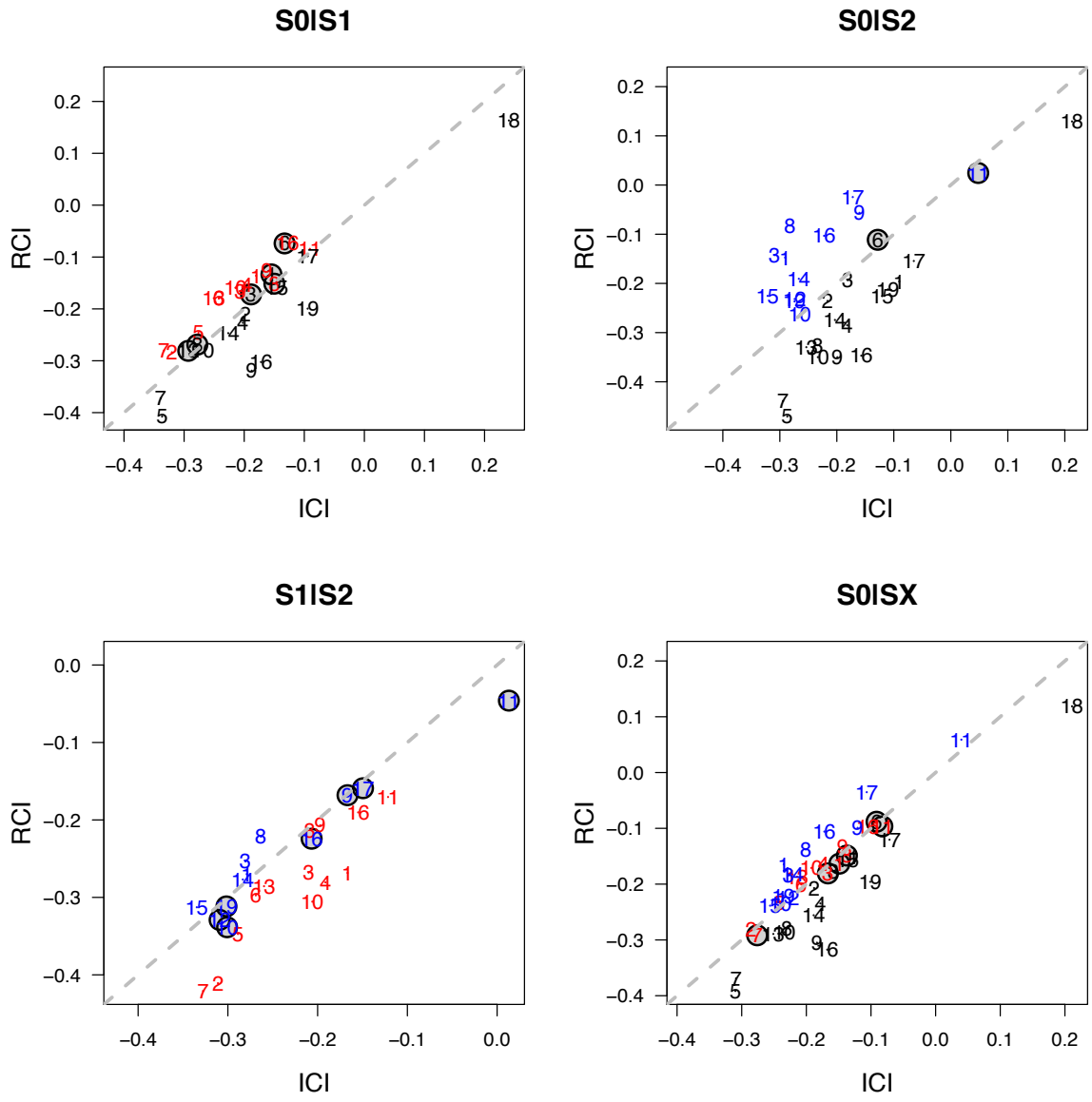

Figure S8: **Comparisons between visually determined hypnograms and fMRI-based predictions.** The EEG based gold standard is depicted with a red line; the fMRI-based prediction uses a sliding window of 96s and the predictions are given in black for the multiclass problem (i.e., all four stages) and blue for the probability score derived from the S0|SX model. For the latter, predicted periods of wakefulness are highlighted in grey based on a probability cutoff of .75 for sleep (SX).

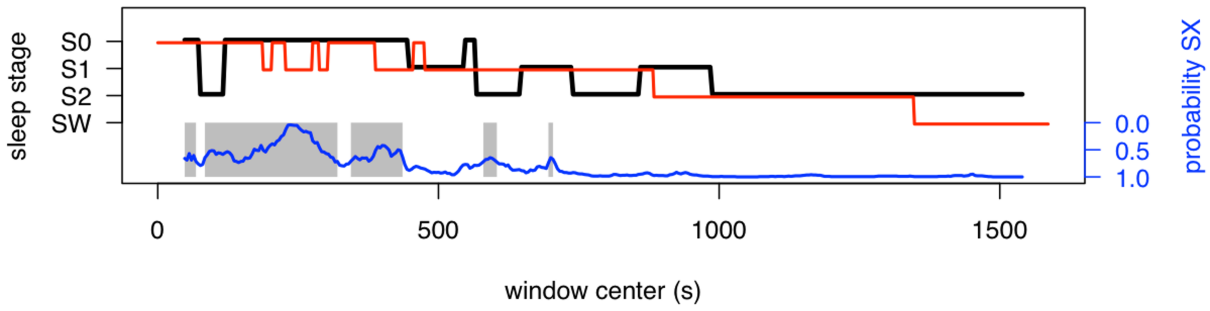

Figure S9: **Difference of the average connection strength between S0 and S1 with global signal retained or regressed out.** When retaining global signal (GS) there is a strong difference in thalamocortical connectivity between S0 and S1 (left two columns in the SC block). It becomes clear that when removing GS, these thalamocortical differences disappear. Nonetheless, a classifier for S0|S1 achieves an AUC of 0.84 in the LOSO-CV on the training data with a 288 s window.

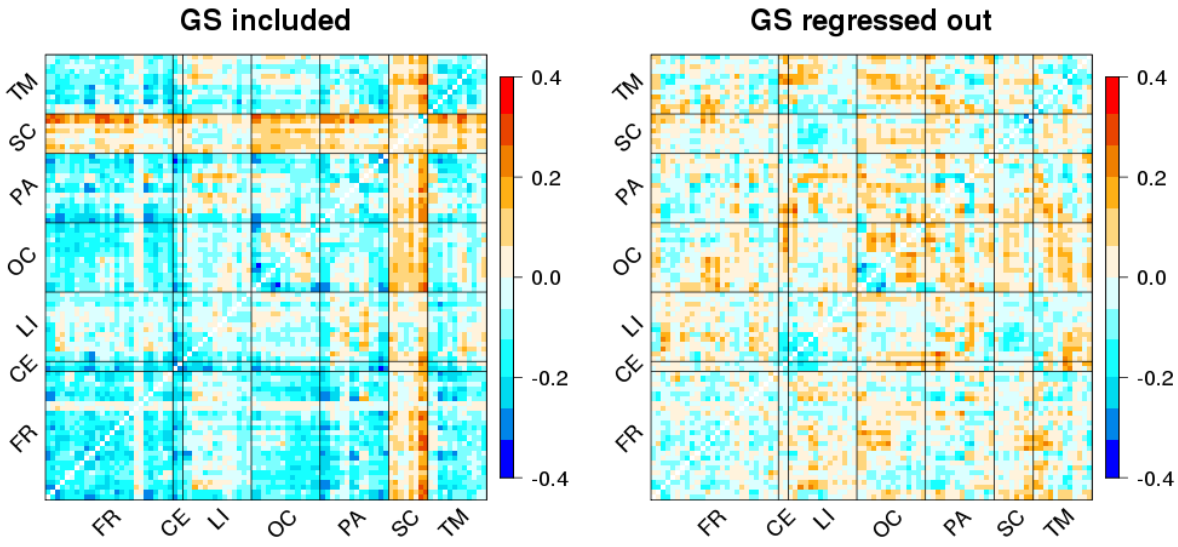

Figure S10: **Application of the classifier to rs-fMRI data recorded during wake and propofol-induced loss of consciousness at a different research center.**

In order to test the sleep classifier performance on data from different acquisition platforms and during different behavioral states, we here use previously published EEG-fMRI data on propofol-induced loss of consciousness (PI-LOC) (Schröter et al. 2012). Although initiated by different cerebral mechanisms, anesthesia has been termed a sleep-like state, and sleep and PI-LOC share remarkable similarities regarding basal cerebral activity pattern, functional connectivity measures and EEG metrics. For example, high density EEG showed that EEG slow waves during PI-LOC are topographically indistinguishable from the ones observed during natural slow-wave sleep, and share similar patterns of origin, propagation and involvement (Murphy et al. 2011). Reduced fMRI connectivity of neocortical regions has been observed by several groups (for a recent review of the literature, see Song and Yu (2015)). Moreover, reduced thalamocortical connectivity is also observed in PI-LOC (Liu et al. 2013; Ni Mhuircheartaigh et al. 2013). Therefore, we expected that our sleep classifier should be able to distinguish wakefulness and PI-LOC.

Each panel in the figure depicts the predicted sleep stage probability for 11 subjects during PI-LOC as well as during wakefulness (awake). The panels differ in the classifier being used. The resulting AUC values range from 0.82 for S0|S1 to 1.0 for S0|SW. The data were recorded at a different research center on different hardware compared to the training dataset, i.e. a Philips 3 Tesla scanner instead of 1.5 Tesla GE, but the preprocessing was similar to the preprocessing used for the training dataset. For further details on fMRI acquisition parameters and preprocessing see Schröter *et al.* (2012). Similar to functional connectivity changes between wakefulness and sleep, the initial rs-fMRI functional connectivity analysis (Schröter *et al.* 2012) found pronounced decreases in thalamocortical connectivity as well as altered cortico-cortical connectivity during deep anesthesia compared to wakefulness.

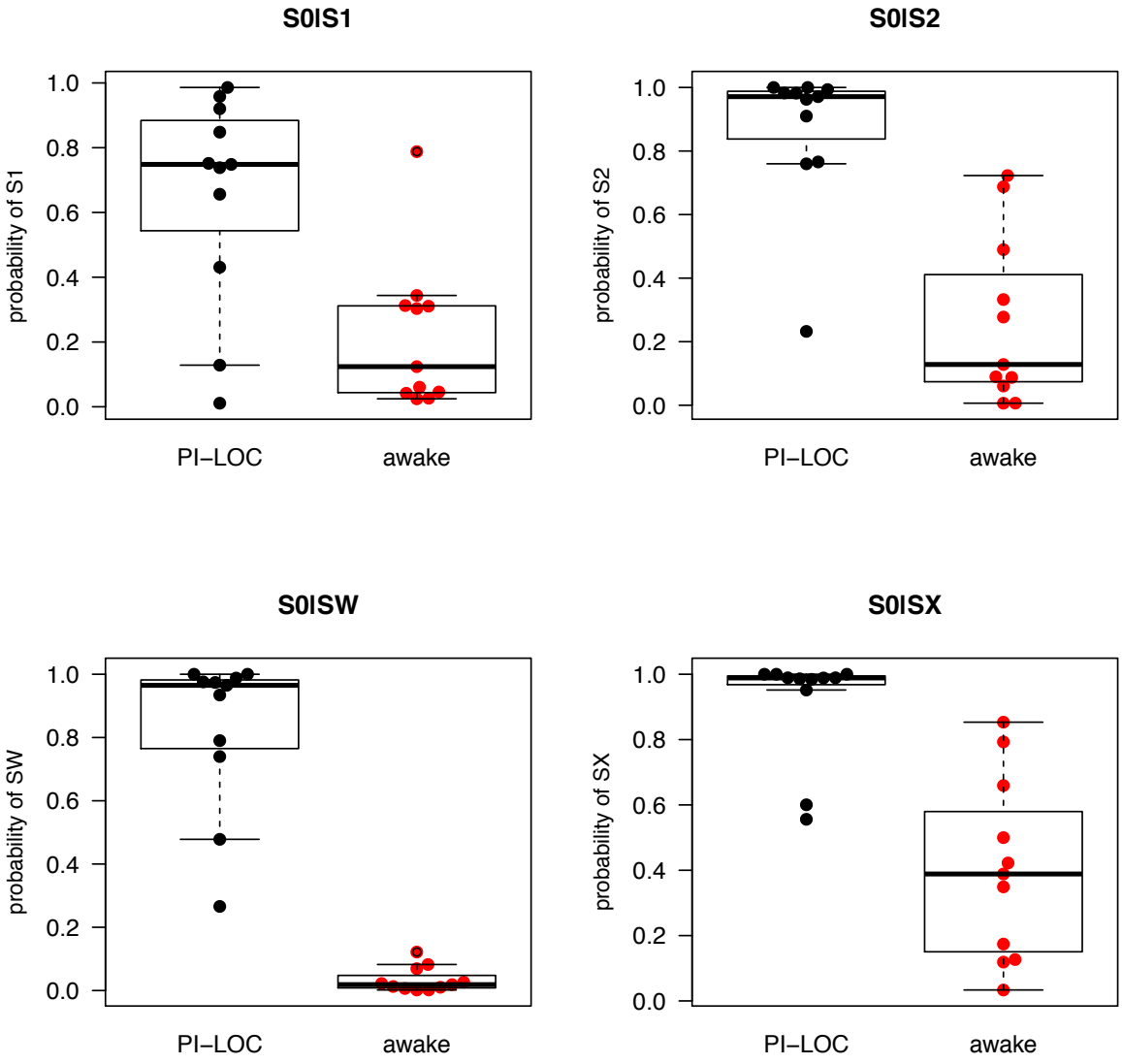
S0IS1
probability of S1
1.0
0.8
0.6
0.4
0.2
0.0
PI–LOC
awake
S0IS2
probability of S2
1.0
0.8
0.6
0.4
0.2
0.0
PI–LOC
awake
S0ISW
probability of SW
1.0
0.8
0.6
0.4
0.2
0.0
PI–LOC
awake
S0ISX
probability of SX
1.0
0.8
0.6
0.4
0.2
0.0
PI–LOC
awake

Table S1: **Selection of 5-minute epochs from individual datasets.**

Training dataset[a]						Validation dataset[b]				
Subject number	**fMRI run**	**S0**	**S1**	**S2**	**SW**	**Subject number**	**fMRI run**	**S0**	**S1**	**S2**
1	1	1	-	-	1	**1**	2	1	1	1
2	1 and 2	-	1	2	3	**2**	1 and 2	1	1	-
3	1	1	1	-	-	**3**	2	1	1	1
4	1, 2 and 3	3	-	2	-	**4**	1 and 2	1	1	-
5	1 and 2	2	2	2	2	**5**	1 and 2	1	-	1
6	1	1	1	-	-	**6**	1 and 2	1	1	-
7	1	1	1	-	-	**7**	2	-	-	1
8	1	1	-	1	-	**8**	1	1	-	-
9	1	2	1	-	-	**9**	1 and 2	1	1	-
10	1	1	1	-	-	**10**	1,2 and 3	1	1	1
11	1 and 2	2	2	-	-	**11**	1 and 2	1	1	-
12	1 and 2	3	2	3	1	**12**	1 and 2	1	-	1
13	1 and 2	1	2	1	-	**13**	1 and 2	1	1	1
14	1 and 2	4	2	-	-	**14**	1 and 2	1	-	1
15	1	-	1	-	-	**15**	2 and 3	1	1	1
16	1	-	1	-	-	**16**	2	-	1	1
17	1 and 2	-	1	3	1	**17**	2 and 3	1	1	-
18	1 and 2	2	1	-	1	**18**	None	-	-	-
19	1	-	1	-	-	**19**	1 and 3	1	-	1
20	1 and 2	2	2	-	-	**20**	1 and 2	1	1	1
21	1 and 2	-	1	-	3					
22	1 and 2	-	-	3	2					
23	1 and 2	-	-	4	1					
24	1	-	-	3	2					
25	1	-	-	-	1					

[a]maximum three runs, each lasting 26.7 minutes

[b]runs consisting of short acquisition (5 minutes) and two long acquisitions (each 24.5 minutes)

Table S2: **Mapping of AAL regions of interest (ROIs) to ROI IDs (#) and lobe**

#	Name	Lobe
1	Precentral gyrus, Left	Frontal
2	Precentral gyrus, Right	Frontal
3	Superior frontal gyrus, Left	Frontal
4	Superior frontal gyrus, Right	Frontal
5	Orbitofrontal cortex (superior), Left	Frontal
6	Orbitofrontal cortex (superior), Right	Frontal
7	Middle Frontal Gyrus, Left	Frontal
8	Middle Frontal Gyrus, Right	Frontal
9	Orbitofrontal cortex (medial), Left	Frontal
10	Orbitofrontal cortex (medial), Right	Frontal
11	Inferior frontal gyrus (opercular), Left	Frontal
12	Inferior frontal gyrus (opercular), Right	Frontal
13	Inferior frontal gyrus (triangular), Left	Frontal
14	Inferior frontal gyrus (triangular), Right	Frontal
15	Orbitofrontal cortex (inferior), Left	Frontal
16	Orbitofrontal cortex (inferior), Right	Frontal
17	Supplementary motor area, Left	Frontal
18	Supplementary motor area, Right	Frontal
19	Olfactory, Left	Frontal
20	Olfactory, Right	Frontal
21	Superior frontal gyrus (medial), Left	Frontal
22	Superior frontal gyrus (medial), Right	Frontal
23	Orbitofrontal cortex (middle), Left	Frontal
24	Orbitofrontal cortex (middle), Right	Frontal
25	Rectus gyrus, Left	Frontal
26	Rectus gyrus, Right	Frontal
27	Rolandic operculum, Left	Central
28	Rolandic operculum, Right	Central
29	Insula, Left	Limbic
30	Insula, Right	Limbic
31	Anterior Cingulate Gyrus, Left	Limbic
32	Anterior Cingulate Gyrus, Right	Limbic
33	Middle Cingulate Gyrus, Left	Limbic
34	Middle Cingulate Gyrus, Right	Limbic
35	Posterior Cingulate Gyrus, Left	Limbic
36	Posterior Cingulate Gyrus, Right	Limbic
37	Hippocampus, Left	Limbic
38	Hippocampus, Right	Limbic
39	Parahippocampus gyrus, Left	Limbic
40	Parahippocampus gyrus, Right	Limbic
41	Amygdala, Left	Limbic
42	Amygdala, Right	Limbic
43	Calcarine Cortex, Left	Occipital
44	Calcarine Cortex, Right	Occipital
45	Cuneus, Left	Occipital

46	Cuneus, Right	Occipital
47	Lingual gyrus, Left	Occipital
48	Lingual gyrus, Right	Occipital
49	Superior occipital gyrus, Left	Occipital
50	Superior occipital gyrus, Right	Occipital
51	Middle occipital gyrus, Left	Occipital
52	Middle occipital gyrus, Right	Occipital
53	Inferior occipital gyrus, Left	Occipital
54	Inferior occipital gyrus, Right	Occipital
55	Fusiform gyrus, Left	Occipital
56	Fusiform gyrus, Right	Occipital
57	Postcentral gyrus, Left	Parietal
58	Postcentral gyrus, Right	Parietal
59	Superior parietal gyrus, Left	Parietal
60	Superior parietal gyrus, Right	Parietal
61	Inferior parietal lobule, Left	Parietal
62	Inferior parietal lobule, Right	Parietal
63	Supramarginal gyrus, Left	Parietal
64	Supramarginal gyrus, Right	Parietal
65	Angular Gyrus, Left	Parietal
66	Angular Gyrus, Right	Parietal
67	Precuneus, Left	Parietal
68	Precuneus, Right	Parietal
69	Paracentral lobule, Left	Parietal
70	Paracentral lobule, Right	Parietal
71	Caudate, Left	Subcortical
72	Caudate, Right	Subcortical
73	Putamen, Left	Subcortical
74	Putamen, Right	Subcortical
75	Pallidum, Left	Subcortical
76	Pallidum, Right	Subcortical
77	Thalamus, Left	Subcortical
78	Thalamus, Right	Subcortical
79	Heschl's gyrus, Left	Temporal
80	Heschl's gyrus, Right	Temporal
81	Superior temporal gyrus, Left	Temporal
82	Superior temporal gyrus, Right	Temporal
83	Temporal pole (superior), Left	Temporal
84	Temporal pole (superior), Right	Temporal
85	Middle temporal gyrus, Left	Temporal
86	Middle temporal gyrus, Right	Temporal
87	Temporal pole (middle), Left	Temporal
88	Temporal pole (middle), Right	Temporal
89	Inferior temporal gyrus, Left	Temporal
90	Inferior temporal gyrus, Right	Temporal

References

Liu X, Lauer KK, Ward BD, Li SJ, Hudetz AG. 2013. Differential effects of deep sedation with propofol on the specific and nonspecific thalamocortical systems: a functional magnetic resonance imaging study. Anesthesiology 118:59-69.

Murphy M, Bruno MA, Riedner BA, Boveroux P, Noirhomme Q, Landsness EC, Brichant JF, Phillips C, Massimini M, Laureys S, Tononi G, Boly M. 2011. Propofol anesthesia and sleep: a high-density EEG study. Sleep 34:283-291A.

Ni Mhuircheartaigh R, Warnaby C, Rogers R, Jbabdi S, Tracey I. 2013. Slow-wave activity saturation and thalamocortical isolation during propofol anesthesia in humans. Science translational medicine 5:208ra148.

Schröter MS, Spoormaker VI, Schorer A, Wohlschlager A, Czisch M, Kochs EF, Zimmer C, Hemmer B, Schneider G, Jordan D, Ilg R. 2012. Spatiotemporal reconfiguration of large-scale brain functional networks during propofol-induced loss of consciousness. The Journal of neuroscience : the official journal of the Society for Neuroscience 32:12832-12840.

Song XX, Yu BW. 2015. Anesthetic effects of propofol in the healthy human brain: functional imaging evidence. Journal of anesthesia 29:279-288.